IEEE Access
Multidisciplinary | Rapid Review | Open Access Journal

Received February 20, 2017, accepted April 5, 2017, date of publication April 13, 2017, date of current version June 7, 2017.

Digital Object Identifier 10.1109/ACCESS.2017.2693288

A Kalman Estimation Based Rao-Blackwellized Particle Filtering for Radar Tracking

JINGXIAN LIU[1], ZULIN WANG[1,2], (Member, IEEE), AND MAI XU[1], (Senior Member, IEEE)
[1]School of Electrical and Information Engineering, Beihang University, Beijing 100191, China
[2]Collaborative Innovation Center of Geospatial Technology, 129 Luoyou Road, Wuhan, China

Corresponding author: Mai Xu (maixu@buaa.edu.cn)

This work was supported in part by NSFC under Grant 61202139, Grant 61573037, and Grant 61471022 and in part by the Fok Ying Tung Education Foundation under Grant 151061.

ABSTRACT The Rao-Blackwellized particle filtering (RBPF) offers a general tracking framework with linear/nonlinear state space models, which outperforms the standard particle filtering in nonlinear and non-Gaussian tracking scenarios. Unfortunately, in conventional radar systems, the observations contain no information about the linear part of target state. In these cases, the RBPF algorithm fails to catch the real trajectories, because we cannot obtain the enough information to correctly update the linear part of target state in the tracking procedure. To overcome such an issue, this paper proposes a Kalman estimation-based BRPF (KE-BRPF) algorithm. In KE-RBPF, the correlation between linear and nonlinear parts of target state is investigated. Benefitting from such investigation, we derive a new set of formulea to present the correlation in terms of means and variances. By utilizing these formulas, our KE-RBPF algorithm correctly tracks the linear part of target state based on the nonlinear one. Finally, the simulation results verify that, our KE-RBPF performs better than other state-of-the-art tracking methods in nonlinear and non-Gaussian radar tracking scenarios, with at least 18% reduction in terms of the means and central tendency of error of tracking root-mean-square-error.

INDEX TERMS Kalman estimation, Rao-Blackwellized particle filtering, central tendency of error.

I. INTRODUCTION

The Bayesian tracking theory [2], [3] is a fundamental structure for tracking with State Space (SS) model [4], which can be simplified into Kalman Filtering (KF) algorithms [5], [6] in the application of tracking with only Gaussian noise. In non-Gaussian tracking scenarios, a common solution, called Particle Filtering (PF) or Standard PF (SPF) [7], was worked out based on the Sequential Monte Carlo sampling [8]. Afterwards, some advanced PF algorithms, such as Unscented PF (UPF) [9], were proposed to improve the tracking performance by utilizing better sampling distributions. However, once the dimensions of target state increase, the computational cost in those PF algorithms becomes extremely expensive, and the tracking performance obviously degrades. To avoid above drawbacks, a Rao-Blackwellized PF (RBPF) [10], which is also called Marginalized PF (MPF) [11], was proposed. RBPF is inspired by the fact that the structure of many SS models is composed of linear and nonlinear parts [12]. Accordingly, in RBPF, KF is utilized to handle the linear part, leaving only the nonlinear part to PF. By this way, the dimension of target state tracked by PF is compressed as much as possible in the RBPF algorithm. As such, the RBPF algorithm reduces the computational resource of the tracking process over PF, thus more practical for real applications. Moreover, RBPF can also improve the tracking performance by reducing its tracking variance [13]. Benefiting from these advantages, the RBPF has been widely used in the fields of simultaneous localization [14], visual tracking [15] and automatic controlling [16], [17]. Recently, some advanced RBPF algorithms have been proposed for the implementation in particle swarm tracking [18], adaptive beamforming with strong interference [19], out-of-sequence measurement processing [20] and other classic tracking and filtering cases [21].

As all we know, the RBPF algorithm separates the estimated state into nonlinear and linear parts, which are calculated with the previous state and present observations. However, the observations in conventional radar systems offer no information about the linear part of target state. For example, many active (or passive) radars locate the target without its velocity [22] that is the linear part of target state in SS models. Unlike visual tracking, we cannot obtain a good tracking

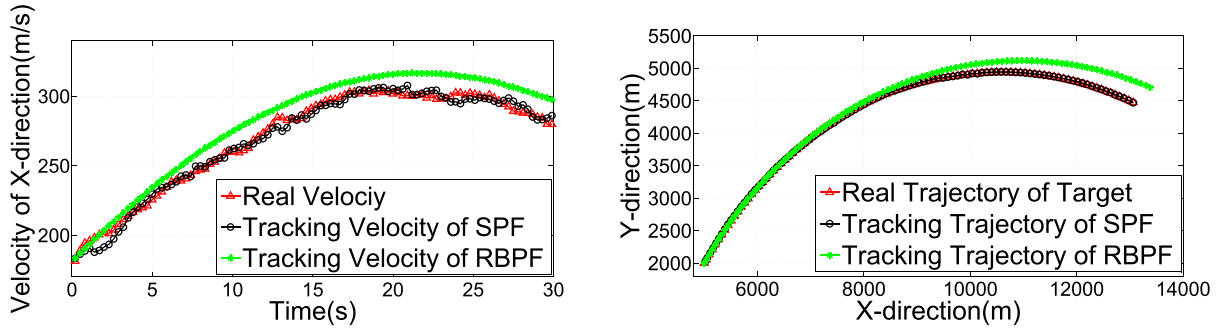

FIGURE 1. Tracking results of RBPF with constant turn model [23], in comparison with SPF. Left figure: The velocities tracked by RBPF and SPF in X direction are shown. Right figure: The tracking trajectories are shown, in which the tracking trajectory of RBPF gradually deviates from the real one.

performance without velocity in radar tracking. To compensate this information loss, [11] utilizes the nonlinear part of the next prediction state as an additional observation of the present linear part. However, this compensation still cannot afford enough information to correctly update the linear part[1] in the aforementioned scenario. Hence, as seen in Figure 1, the velocity tracked by RBPF is too smooth to catch the real one and causes a gradual deviation of the tracking trajectory.

To our best knowledge, few methods are proposed to overcome this gradual deviation problem in RBPF while observations contain no information about the linear part of target state. Hence, in this paper, a Kalman Estimation based RBPF (KE-RBPF) algorithm is proposed to solve this problem for the first time. Specifically, by investigating the Kalman estimation procedure, the correlation between linear and nonlinear parts of target state is formulated with an equation set in the form of mean and variance. Benefitting from such a formulation, the linear part can be correctly estimated, according to the mean and variance of the nonlinear part at each time step. Finally, the simulational results verify that our KE-RBPF algorithm outperforms other classic nonlinear non-Gaussian tracking algorithms, in terms of means, deviations, and central tendency of error (CTE) [24], [25]. The meanings of notation in the paper are listed in Table 1. The contributions of this paper are listed as follows,

- We investigate the tracking degradation of RBPF when the observation information on the linear part is unavailable.
- We propose a novel KE-RBPF to overcome the degradation of RBPF in tracking by formulating the correlation between linear and nonlinear parts of target state with an equation set.

II. RAO-BLACKWELLIZED PARTICLE FILTERING FOR RADAR TRACKING

This section investigates the degradation of RBPF tracking performance in the radar tracking systems without the observation information on the linear part. The linear/nonlinear

[1]This problem is further discussed in Section II

Algorithm 1 RBPF for Radar Tracking Without the Observation Information on the Linear Part

Input: $N \in \mathbb{N}_+$, the prior probability p_0 of $\boldsymbol{x}^n$, the mean $\bar{\boldsymbol{x}}_0^l$ and variance $\bar{\boldsymbol{P}}_0^{ll}$ of $\boldsymbol{x}^l$, the tracking model (1).

Output: $\{[\boldsymbol{x}_{k|k}^{n,(i)}, \boldsymbol{x}_{k|k}^{l,(i)}]^{\mathrm{T}}\}_{i=1}^N$, at time step k.

Initialize: for $i = 1, 2, ..., N$, draw particle $\boldsymbol{x}_{1|0}^{n,(i)} \sim p_0$ with the set $\{\boldsymbol{x}_{1|0}^{l,(i)}, \boldsymbol{P}_{1|0}^{ll,(i)}\} = \{\bar{\boldsymbol{x}}_0^l, \bar{\boldsymbol{P}}_0^{ll}\}$, and the weight $w_0^{(i)} = 1/N$.

For: time step $k = 1, 2, 3....$

1: Weight update: for $i = 1, ..., N$, given observation $\boldsymbol{z}_k$, $w_k^{(i)} = \frac{p(\boldsymbol{z}_k|\boldsymbol{x}_{k|k-1}^{n,(i)})}{C_k} w_{k-1}^{(i)}$, where C_k is the normalized constant.

2: Particle update: for $i = 1, ..., N$, particle unchange, i.e.,$\boldsymbol{x}_{k|k}^{n,(i)} = \boldsymbol{x}_{k|k-1}^{n,(i)}$, and $\{\boldsymbol{x}_{k|k}^{l,(i)}, \boldsymbol{P}_{k|k}^{ll,(i)}\} = \{\boldsymbol{x}_{k|k-1}^{l,(i)}, \boldsymbol{P}_{k|k-1}^{ll,(i)}\}$.

3: Particles resampling (optional).

4: Nonlinear state prediction: for $i = 1, ..., N$, draw new particle $\boldsymbol{x}_{k+1|k}^{n,(i)} \sim p(\boldsymbol{x}_{k+1|k}^n|\boldsymbol{x}_{k|k}^{(i)})$.

5: Linear state prediction: for $i = 1, ..., N$, $\boldsymbol{x}_{k+1|k}^{l,(i)}$ and $\boldsymbol{P}_{k+1|k}^{ll,(i)}$ are calculated with the Kalman Filtering algorithm with decorrelating process [11], given SS model (1), $\boldsymbol{x}_{k|k}^{l,(i)}$, $\boldsymbol{P}_{k|k}^{ll,(i)}$ and $\boldsymbol{z}_k^{a,(i)}$, where

$$\boldsymbol{z}_k^{a,(i)} = \boldsymbol{x}_{k+1|k}^{n,(i)} - \boldsymbol{F}^{nn}\boldsymbol{x}_{k|k}^{n,(i)}. \tag{2}$$

End

SS model [11] of aforementioned radar tracking systems is defined as follows,

$$\boldsymbol{x}_k^n = \boldsymbol{F}^{nn}\boldsymbol{x}_{k-1}^n + \boldsymbol{F}^{nl}\boldsymbol{x}_{k-1}^l + \boldsymbol{v}_{k-1}^n \tag{1a}$$
$$\boldsymbol{x}_k^l = \boldsymbol{F}^{ln}\boldsymbol{x}_{k-1}^n + \boldsymbol{F}^{ll}\boldsymbol{x}_{k-1}^l + \boldsymbol{v}_{k-1}^l \tag{1b}$$
$$\boldsymbol{z}_k = \boldsymbol{h}(\boldsymbol{x}_k^n) + \boldsymbol{w}_k^n, \tag{1c}$$

where k is the tracking time. In (1), $\{\boldsymbol{x}_k^n; \boldsymbol{x}_k^n \in \mathbb{R}^{d_{x^n}}\}$ is the nonlinear part of target state with dimension d_{x^n}, while $\{\boldsymbol{x}_k^l; \boldsymbol{x}_k^l \in \mathbb{R}^{d_{x^l}}\}$ is the linear part with dimension d_{x^l}. $\boldsymbol{z}_k$ is observation result. $\boldsymbol{F}^{nn}$, $\boldsymbol{F}^{nl}$, $\boldsymbol{F}^{ln}$ and $\boldsymbol{F}^{ll}$ are state transition

TABLE 1. Notation list.

notation	meaning of the notation
k	discrete time step for tracking, $k = 1, 2, 3, ...$
$\boldsymbol{x}_k$	target state vector at time step k, containing linear part $\boldsymbol{x}_k^l$ and nonlinear part $\boldsymbol{x}_k^n$, i.e., $\boldsymbol{x}_k = [(\boldsymbol{x}_k^n)^{\mathrm{T}} \quad (\boldsymbol{x}_k^l)^{\mathrm{T}}]^{\mathrm{T}}$.
$\hat{\boldsymbol{x}}_{k\|k-1}$, $\hat{\boldsymbol{x}}_{k\|k}$	prediction and updating state vectors of $\boldsymbol{x}_k$, respectively.
$\boldsymbol{P}_k$	variance matrix of state vector at time step k.
$\boldsymbol{P}_k^{ll}$, $\boldsymbol{P}_k^{nn}$	variance matrices of state vector of linear and nonlinear parts at time step k, respectively.
$\boldsymbol{P}_k^{nl}$, $\boldsymbol{P}_k^{ln}$	covariance matrices of state vector for linear and nonlinear parts at time step k..
$\boldsymbol{P}_{k\|k-1}$, $\boldsymbol{P}_{k\|k}$	prediction and updating variance matrices of $\boldsymbol{x}_k$, respectively. The corresponding denotations of other matrices have the same meaning in this paper.
$\boldsymbol{F}^{nn}$, $\boldsymbol{F}^{nl}$, $\boldsymbol{F}^{ln}$ and $\boldsymbol{F}^{ll}$	the state transition matrices.
$\boldsymbol{v}_{k-1}^l$, $\boldsymbol{v}_{k-1}^n$	transition noises of linear and nonlinear parts at time step k-1, respectively.
$\boldsymbol{Q}_{k-1}^{ll}$, $\boldsymbol{Q}_{k-1}^{nn}$	variance matrices of $\boldsymbol{v}_{k-1}^l$ and $\boldsymbol{v}_{k-1}^n$, respectively.
$\boldsymbol{z}_k$	observation vector at time step k.
$\boldsymbol{h}(\cdot)$	nonlinear observation function.
$\boldsymbol{H}$, $\boldsymbol{H}^l$, $\boldsymbol{H}^n$	observation matrices for state vectors $\boldsymbol{x}_k$, $\boldsymbol{x}_k^l$ and $\boldsymbol{x}_k^n$.
$\boldsymbol{w}_k^n$	observation noise at time k, which can be non-Gaussian.
$(\cdot)^{(i)}$	corresponding vectors, variances, or covariances of the i-th particle.
N	number of particles.
$w_k^{(i)}$	weight of the i-th particle at time step k.
$p(\cdot)$	distribution function.
$\boldsymbol{O}$	zero matrix.
$d_{x,k}, d_{y,k}$	distances along x and y direction at time step k.
$v_{x,k}, v_{y,k}$	velocity along x and y direction at time step k.
α	turn rate in constant turn model.
s_T	sampling interval.
v_d, v_v	transition noise of distance and velocity.
θ_k, r_k	observation value of azimuth and distance.
ϵ	glint noise probability.
w_θ, w_r	observation noise of azimuth and distance.

matrices. $\boldsymbol{v}_{k-1}^n \sim \mathcal{N}(0, \boldsymbol{Q}_{k-1}^{nn})$ and $\boldsymbol{v}_{k-1}^l \sim \mathcal{N}(0, \boldsymbol{Q}_{k-1}^{ll})$ are transition noises with zero means, and their variances are $\boldsymbol{Q}_{k-1}^{nn}$ and $\boldsymbol{Q}_{k-1}^{ll}$, respectively. In (1c), $\boldsymbol{h}(\cdot)$ is a nonlinear observation function with arbitrary observation noise $\boldsymbol{w}_k^n$, which obeys Gaussian or non-Gaussian distribution. Based on (1), the detail of the RBPF [11] for conventional radar tracking is shown in Algorithm 1.

As seen in this algorithm, at time step k, each particle $\boldsymbol{x}_{k|k}^{(i)}$ contains nonlinear and linear parts, i.e., $\boldsymbol{x}_{k|k}^{(i)} \triangleq [\boldsymbol{x}_{k|k}^{n,(i)}, \boldsymbol{x}_{k|k}^{l,(i)}]^{\mathrm{T}}$, which are estimated by PF and KF, respectively. For both PF and KF tracking procedures, the states are updated first given observation $\boldsymbol{z}_k$, and then they are predicted with SS model of (1).[2] In fact, there is normally no real observation about the linear part of target state in the conventional radar tracking procedure. Specifically, we cannot specify a linear transition matrix for the linear part of state in the observation function of (1c). Hence, we cannot calculate the Kalman gain for updating this linear part $\boldsymbol{x}_{k|k}^{l,(i)}$, which should only be directly replaced by the previous prediction $\boldsymbol{x}_{k|k-1}^{l,(i)}$ as seen at the second step of Algorithm 1. A compensation in RBPF for updating the linear part of target state is that a new variable $z_k^{a,(i)}$ calculated by (2) is utilized as an additional observation of $\boldsymbol{x}_{k|k}^{l,(i)}$. Note that $\boldsymbol{x}_{k+1|k}^{n,(i)}$ is the prediction of the nonlinear part in the i-th particle, which is drawn from $p(\boldsymbol{x}_{k+1|k}^n|\boldsymbol{x}_{k|k}^{(i)})$ by a prediction process in [26]. However, according to the SS model (1) and the procedure of Rao-Blackwellisation [11], [27], $p(\boldsymbol{x}_{k+1|k}^n|\boldsymbol{x}_{k|k}^{(i)})$ is in fact calculated as follows,

$$p(\boldsymbol{x}_{k+1|k}^n|\boldsymbol{x}_{k|k}^{(i)}) = \mathcal{N}(\boldsymbol{F}^{nn}\boldsymbol{x}_{k|k}^{n,(i)} + \boldsymbol{F}^{nl}\boldsymbol{x}_{k|k}^{l,(i)}, \boldsymbol{F}^{nl}\boldsymbol{P}_{k|k}^{ll,(i)}(\boldsymbol{F}^{nl})^{\mathrm{T}} + \boldsymbol{Q}_k^{nn}). \tag{3}$$

Obviously, in (3), each prediction in particle obeys

$$\boldsymbol{x}_{k+1|k}^{n,(i)} = \boldsymbol{F}^{nn}\boldsymbol{x}_{k|k}^{n,(i)} + \boldsymbol{F}^{nl}\boldsymbol{x}_{k|k}^{l,(i)} + \sigma, \tag{4}$$

where σ denotes Gaussian noise with variance of $\boldsymbol{F}^{nl}\boldsymbol{P}_{k|k}^{ll,(i)}(\boldsymbol{F}^{nl})^{\mathrm{T}} + \boldsymbol{Q}_k^{nn}$. We derive $z_k^{a,(i)}$ from (2) and (4),

$$z_k^{a,(i)} = \boldsymbol{F}^{nl}\boldsymbol{x}_{k|k}^{l,(i)} + \sigma. \tag{5}$$

[2]These procedures are different from our KE-RBPF which predicts the target state first then updates it. These differences do not essentially affect the tracking performance except a little diversity of tracking results in the beginning of tracking, which is further discussed in Section IV.

With the direct correlation of nonlinear and linear part in SS model, we can derive the additional observation for linear part in (2). However, (5) implies that this additional observation has no correlation with real observation z_k. Hence, we obtain no information from observation $z_k^{a,(i)}$ to update the linear state variable $\boldsymbol{x}_k^l$, but only the partial state transition matrix $\boldsymbol{F}^{nl}$. This drawback causes the case, as seen in Figure 1, that the velocity tracked by RBPF is smooth, without catching any information on real observation z_k as SPF works. As a result, RBPF incurs the gradual deviation of tracking trajectory from real one, thus degrading the tracking performance in the radar tracking systems without observation information on the linear part.

III. KALMAN ESTIMATION BASED RAO-BLACKWELLIZED PARTICLE FILTERING

In this section, a novel KE-RBPF is proposed to solve the aforementioned deviation problem of RBPF algorithm in Section II. Normally, the goal of tracking [10] is to obtain the expectation[3] $I(f_n)$ based on the conditional distribution as follows,

$$I(f_n) = \int\int f_n(\boldsymbol{x}_k^n, \boldsymbol{x}_k^l) p(\boldsymbol{x}_k^n, \boldsymbol{x}_k^l | z_{1:k}) d\boldsymbol{x}_k^l d\boldsymbol{x}_k^n. \tag{6}$$

Obviously, from (6), we can derive

$$\begin{aligned} &I(f_n) \\ &= \int\int f_n(\boldsymbol{x}_k^n, \boldsymbol{x}_k^l)[p(\boldsymbol{x}_k^n|z_{1:k}) p(\boldsymbol{x}_k^l|\boldsymbol{x}_k^n, z_{1:k})] d\boldsymbol{x}_k^l d\boldsymbol{x}_k^n \\ &= \int \underbrace{[\int f_n(\boldsymbol{x}_k^n, \boldsymbol{x}_k^l) p(\boldsymbol{x}_k^l|\boldsymbol{x}_k^n, z_{1:k}) d\boldsymbol{x}_k^l]}_{\textbf{Correlation}} \underbrace{p(\boldsymbol{x}_k^n|z_{1:k})}_{\textbf{SPF}} d\boldsymbol{x}_k^n. \end{aligned} \tag{7}$$

(7) implies that, as soon as we formulate an equation set for the correlation, we can utilize the statistical characteristics of nonlinear part $\boldsymbol{x}_k^n$ to estimate the ones of linear, based on the RBPF procedure, thus achieving correct tracking results. However, the traditional RBPF method only uses the SS model to derive the correlation, seen in (2) of Algorithm 1. Obviously, this correlation only contains the information of the predicted state $\boldsymbol{x}_{k+1|k}^{n,(i)}$, neglecting the variance information between nonlinear and linear parts. This problem leads to the loss of observation information, as mentioned in Section II. To conquer this problem, our KE-RBPF uses the Kalman estimation procedure [5] to formulate an equation set for the correlation between $\boldsymbol{x}_k^n$ and $\boldsymbol{x}_k^l$ in (7), such that both $\boldsymbol{x}_k^l$ and its variance $\boldsymbol{P}_k^l$ can be correctly estimated through the nonlinear part. The final tracking procedure of our KE-RBPF is presented as follows. First, based on the nonlinear part of linear/nonlinear models, the estimation results of nonlinear part are calculated by standard PF. Then, we utilize these results to estimate the linear part with the equation set of correlation formulated by Kalman estimation procedure, thus obtaining the whole tracking results in our KE-RBPF algorithm.

[3]The expectation can be the mean or variance of state variable.

To achieve the Kalman estimation procedure, we need to combine the linear and nonlinear parts of target state together. Then, the Kalman filtering is carried out with prediction and update steps, in which we formulate an equation set of the correlation in the form of mean and variance. Specifically, in our linear/nonlinear model (1), we have the following definition to integrate the transition matrix, state vectors and their variances into a conventional SS model:

$$\begin{aligned} \boldsymbol{F} &= \begin{bmatrix} \boldsymbol{F}^{nn} & \boldsymbol{F}^{nl} \\ \boldsymbol{F}^{ln} & \boldsymbol{F}^{ll} \end{bmatrix}, \quad \boldsymbol{Q}_{k-1} = \begin{bmatrix} \boldsymbol{Q}_{k-1}^{nn} & \boldsymbol{Q}_{k-1}^{nl} \\ \boldsymbol{Q}_{k-1}^{ln} & \boldsymbol{Q}_{k-1}^{ll} \end{bmatrix}, \\ \hat{\boldsymbol{x}}_{k-1|k-1} &= \begin{bmatrix} \hat{\boldsymbol{x}}_{k-1|k-1}^n \\ \hat{\boldsymbol{x}}_{k-1|k-1}^l \end{bmatrix}, \quad \boldsymbol{v}_{k-1} = \begin{bmatrix} \boldsymbol{v}_{k-1}^n \\ \boldsymbol{v}_{k-1}^l \end{bmatrix}, \\ \boldsymbol{P}_{k-1|k-1} &= \begin{bmatrix} \boldsymbol{P}_{k-1|k-1}^{nn} & \boldsymbol{P}_{k-1|k-1}^{nl} \\ \boldsymbol{P}_{k-1|k-1}^{ln} & \boldsymbol{P}_{k-1|k-1}^{ll} \end{bmatrix}, \end{aligned} \tag{8}$$

where $\hat{\boldsymbol{x}}_{k-1|k-1}$ and $\boldsymbol{P}_{k-1|k-1}$ are the mean and variance of previous estimation. Specifically, we have

$$\boldsymbol{Q}_{k-1}^{nl} = \boldsymbol{v}_{k-1}^n (\boldsymbol{v}_{k-1}^l)^{\mathrm{T}} = (\boldsymbol{Q}_{k-1}^{ln})^{\mathrm{T}}, \tag{9}$$

and

$$\begin{aligned} \boldsymbol{P}_{k-1|k-1}^{nl} &= (\boldsymbol{x}_{k-1}^n - \hat{\boldsymbol{x}}_{k-1|k-1}^n)(\boldsymbol{x}_{k-1}^l - \hat{\boldsymbol{x}}_{k-1|k-1}^l)^{\mathrm{T}} \\ &= (\boldsymbol{P}_{k-1|k-1}^{ln})^{\mathrm{T}}, \end{aligned} \tag{10}$$

where $[\cdot]^{\mathrm{T}}$ denotes the transpose operator of the matrix. According to the Kalman estimation procedure, the prediction for target state is given in the following,

$$\hat{\boldsymbol{x}}_{k|k-1} = \boldsymbol{F}\hat{\boldsymbol{x}}_{k-1|k-1} \tag{11a}$$

$$\boldsymbol{P}_{k|k-1} = \boldsymbol{F}\boldsymbol{P}_{k-1|k-1}\boldsymbol{F}^{\mathrm{T}} + \boldsymbol{Q}_{k-1}. \tag{11b}$$

Based on (8) and (11), we have the integrated prediction as follows,

$$\begin{bmatrix} \hat{\boldsymbol{x}}_{k|k-1}^n \\ \hat{\boldsymbol{x}}_{k|k-1}^l \end{bmatrix} = \begin{bmatrix} \boldsymbol{F}^{nn} & \boldsymbol{F}^{nl} \\ \boldsymbol{F}^{ln} & \boldsymbol{F}^{ll} \end{bmatrix} \cdot \begin{bmatrix} \hat{\boldsymbol{x}}_{k-1|k-1}^n \\ \hat{\boldsymbol{x}}_{k-1|k-1}^l \end{bmatrix}, \tag{12}$$

$$\begin{bmatrix} \boldsymbol{P}_{k|k-1}^{nn} & \boldsymbol{P}_{k|k-1}^{nl} \\ \boldsymbol{P}_{k|k-1}^{ln} & \boldsymbol{P}_{k|k-1}^{ll} \end{bmatrix} = \begin{bmatrix} \boldsymbol{F}^{nn} & \boldsymbol{F}^{nl} \\ \boldsymbol{F}^{ln} & \boldsymbol{F}^{ll} \end{bmatrix} \cdot \begin{bmatrix} \boldsymbol{P}_{k-1|k-1}^{nn} & \boldsymbol{P}_{k-1|k-1}^{nl} \\ \boldsymbol{P}_{k-1|k-1}^{ln} & \boldsymbol{P}_{k-1|k-1}^{ll} \end{bmatrix} \cdot \begin{bmatrix} \boldsymbol{F}^{nn} & \boldsymbol{F}^{nl} \\ \boldsymbol{F}^{ln} & \boldsymbol{F}^{ll} \end{bmatrix}^{\mathrm{T}} + \begin{bmatrix} \boldsymbol{Q}_{k-1}^{nn} & \boldsymbol{Q}_{k-1}^{nl} \\ \boldsymbol{Q}_{k-1}^{ln} & \boldsymbol{Q}_{k-1}^{ll} \end{bmatrix}. \tag{13}$$

Upon (12) and (13), the prediction for linear part of target sate is derived as follows,

$$\hat{\boldsymbol{x}}_{k|k-1}^l = \boldsymbol{F}^{ln}\hat{\boldsymbol{x}}_{k-1|k-1}^n + \boldsymbol{F}^{ll}\hat{\boldsymbol{x}}_{k-1|k-1}^l, \tag{14}$$

$$\begin{aligned} \boldsymbol{P}_{k|k-1}^{ll} = {} & \boldsymbol{F}^{ln}\boldsymbol{P}_{k-1|k-1}^{nn}(\boldsymbol{F}^{ln})^{\mathrm{T}} + \boldsymbol{F}^{ll}\boldsymbol{P}_{k-1|k-1}^{ln}(\boldsymbol{F}^{ln})^{\mathrm{T}} \\ & + \boldsymbol{F}^{ln}\boldsymbol{P}_{k-1|k-1}^{nl}(\boldsymbol{F}^{ll})^{\mathrm{T}} \\ & + \boldsymbol{F}^{ll}\boldsymbol{P}_{k-1|k-1}^{ll}(\boldsymbol{F}^{ll})^{\mathrm{T}} + \boldsymbol{Q}_{k-1}^{ll}, \end{aligned} \tag{15}$$

$$\begin{aligned} \boldsymbol{P}_{k|k-1}^{ln} = {} & \boldsymbol{F}^{ln}\boldsymbol{P}_{k-1|k-1}^{nn}(\boldsymbol{F}^{nn})^{\mathrm{T}} + \boldsymbol{F}^{ll}\boldsymbol{P}_{k-1|k-1}^{ln}(\boldsymbol{F}^{nn})^{\mathrm{T}} \\ & + \boldsymbol{F}^{ln}\boldsymbol{P}_{k-1|k-1}^{nl}(\boldsymbol{F}^{nl})^{\mathrm{T}} \\ & + \boldsymbol{F}^{ll}\boldsymbol{P}_{k-1|k-1}^{ll}(\boldsymbol{F}^{nl})^{\mathrm{T}} + \boldsymbol{Q}_{k-1}^{ln}. \end{aligned} \tag{16}$$

$$\begin{aligned}\boldsymbol{P}^{nl}_{k|k-1} &= \boldsymbol{F}^{nn}\boldsymbol{P}^{nn}_{k-1|k-1}(\boldsymbol{F}^{ln})^{\mathrm{T}} + \boldsymbol{F}^{nl}\boldsymbol{P}^{ln}_{k-1|k-1}(\boldsymbol{F}^{ln})^{\mathrm{T}} \\ &\quad + \boldsymbol{F}^{nn}\boldsymbol{P}^{nl}_{k-1|k-1}(\boldsymbol{F}^{ll})^{\mathrm{T}} \\ &\quad + \boldsymbol{F}^{nl}\boldsymbol{P}^{ll}_{k-1|k-1}(\boldsymbol{F}^{ll})^{\mathrm{T}} + \boldsymbol{Q}^{nl}_{k-1}. \end{aligned} \tag{17}$$

Obviously, we have $\boldsymbol{P}^{nl}_{k|k-1} = (\boldsymbol{P}^{ln}_{k|k-1})^{\mathrm{T}}$.

Lemma 1: Given the linear/nonlinear SS model (1), the correlation between $\boldsymbol{x}^n_k$ and $\boldsymbol{x}^l_k$ in the update step can be calculated as follows,

$$\hat{\boldsymbol{x}}^l_{k|k} = \hat{\boldsymbol{x}}^l_{k|k-1} + \boldsymbol{M}_k(\hat{\boldsymbol{x}}^n_{k|k} - \hat{\boldsymbol{x}}^n_{k|k-1}), \tag{18}$$

$$\boldsymbol{P}^{ll}_{k|k} = \boldsymbol{P}^{ll}_{k|k-1} + \boldsymbol{M}_k(\boldsymbol{P}^{nn}_{k|k} - \boldsymbol{P}^{nn}_{k|k-1})(\boldsymbol{M}_k)^{\mathrm{T}}, \tag{19}$$

$$\boldsymbol{P}^{nl}_{k|k} = \boldsymbol{P}^{nn}_{k|k}(\boldsymbol{M}_k)^{\mathrm{T}} = (\boldsymbol{P}^{ln}_{k|k})^{\mathrm{T}}, \tag{20}$$

where $\boldsymbol{M}_k = \boldsymbol{P}^{ln}_{k|k-1}(\boldsymbol{P}^{nn}_{k|k-1})^{-1}$.

Proof: We combine the nonlinear part $\boldsymbol{x}^n_k$ and linear part $\boldsymbol{x}^l_k$ into a whole state $\boldsymbol{x}_k$ for the Kalman estimation processing, i.e., $\boldsymbol{x}_k = [(\boldsymbol{x}^n_k)^{\mathrm{T}}\ (\boldsymbol{x}^l_k)^{\mathrm{T}}]^{\mathrm{T}}$. To simplify the derivation, we use a linear approximation to replace (1c) as $\boldsymbol{z}_k = \boldsymbol{H}\boldsymbol{x}_k + \boldsymbol{w}_k$,[4] by defining $\boldsymbol{H} = \begin{bmatrix}\boldsymbol{H}^n\ \boldsymbol{H}^l\end{bmatrix}$, $\boldsymbol{w} = \begin{bmatrix}\boldsymbol{w}^n\end{bmatrix}$, where, $\boldsymbol{H}^l \equiv \boldsymbol{O}$.

According to the Kalman estimation procedure [5], given (8), the Kalman gain can be derived as follows,

$$\boldsymbol{K} = \begin{bmatrix}\boldsymbol{P}^{nn}_{k|k-1}(\boldsymbol{H}^n)^{\mathrm{T}}\boldsymbol{S}^{-1} \\ \boldsymbol{P}^{ln}_{k|k-1}(\boldsymbol{H}^n)^{\mathrm{T}}\boldsymbol{S}^{-1}\end{bmatrix} \triangleq \begin{bmatrix}\boldsymbol{K}^{nn} \\ \boldsymbol{K}^{ln}\end{bmatrix}, \tag{21}$$

where $\boldsymbol{S} = \boldsymbol{H}^n\boldsymbol{P}^{nn}_{k|k-1}(\boldsymbol{H}^n)^{\mathrm{T}} + \boldsymbol{R}_k$, and $\boldsymbol{R}_k$ is the variance of observation noise $\boldsymbol{w}_k$. Given the observation $\boldsymbol{z}_k$, at time k, we can further derive

$$\begin{bmatrix}\hat{\boldsymbol{x}}^n_{k|k} \\ \hat{\boldsymbol{x}}^l_{k|k}\end{bmatrix} = \begin{bmatrix}\hat{\boldsymbol{x}}^n_{k|k-1} \\ \hat{\boldsymbol{x}}^l_{k|k-1}\end{bmatrix} + \begin{bmatrix}\boldsymbol{K}^{nn}\tilde{\boldsymbol{z}}_k \\ \boldsymbol{K}^{ln}\tilde{\boldsymbol{z}}_k\end{bmatrix}, \tag{22}$$

and

$$\boldsymbol{P}_{k|k} = \boldsymbol{P}_{k|k-1} - \begin{bmatrix}\boldsymbol{K}^{nn}\boldsymbol{S}(\boldsymbol{K}^{nn})^{\mathrm{T}} & \boldsymbol{K}^{nn}\boldsymbol{S}(\boldsymbol{K}^{ln})^{\mathrm{T}} \\ \boldsymbol{K}^{ln}\boldsymbol{S}(\boldsymbol{K}^{nn})^{\mathrm{T}} & \boldsymbol{K}^{ln}\boldsymbol{S}(\boldsymbol{K}^{ln})^{\mathrm{T}}\end{bmatrix}, \tag{23}$$

where $\tilde{\boldsymbol{z}}_k \triangleq \boldsymbol{z}_k - \boldsymbol{H}\hat{\boldsymbol{x}}^n_{k|k-1}$. Moreover, based on (21), the following equations hold,

$$\begin{aligned}&\boldsymbol{P}^{nn}_{k|k-1}(\boldsymbol{H}^n)^{\mathrm{T}}\boldsymbol{S}^{-1} = \boldsymbol{K}^{nn} \\ \Rightarrow\ &(\boldsymbol{H}^n)^{\mathrm{T}}\boldsymbol{S}^{-1} = (\boldsymbol{P}^{nn}_{k|k-1})^{-1}\boldsymbol{K}^{nn},\end{aligned} \tag{24}$$

and

$$\begin{aligned}&\boldsymbol{P}^{ln}_{k|k-1}(\boldsymbol{H}^n)^{\mathrm{T}}\boldsymbol{S}^{-1} = \boldsymbol{K}^{ln} \\ \Rightarrow\ &(\boldsymbol{P}^{ln}_{k|k-1})^{-1}\boldsymbol{K}^{ln} = (\boldsymbol{H}^n)^{\mathrm{T}}\boldsymbol{S}^{-1}.\end{aligned} \tag{25}$$

Hence, we have

$$(\boldsymbol{P}^{ln}_{k|k-1})^{-1}\boldsymbol{K}^{ln} = (\boldsymbol{H}^n)^{\mathrm{T}}\boldsymbol{S}^{-1} = (\boldsymbol{P}^{nn}_{k|k-1})^{-1}\boldsymbol{K}^{nn}. \tag{26}$$

Then, from (21) to (26), the estimations at the update step for mean and variance are derived in the following,

$$\begin{aligned}\hat{\boldsymbol{x}}^l_{k|k} &= \hat{\boldsymbol{x}}^l_{k|k-1} + \boldsymbol{K}^{ln}\tilde{\boldsymbol{z}}_k \\ &= \hat{\boldsymbol{x}}^l_{k|k-1} + \boldsymbol{P}^{ln}_{k|k-1}(\boldsymbol{P}^{nn}_{k|k-1})^{-1}\boldsymbol{K}^{nn}\tilde{\boldsymbol{z}}_k \\ &= \hat{\boldsymbol{x}}^l_{k|k-1} + \boldsymbol{P}^{ln}_{k|k-1}(\boldsymbol{P}^{nn}_{k|k-1})^{-1}(\hat{\boldsymbol{x}}^n_{k|k} - \hat{\boldsymbol{x}}^n_{k|k-1}) \\ &= \hat{\boldsymbol{x}}^l_{k|k-1} + \boldsymbol{M}_k(\hat{\boldsymbol{x}}^n_{k|k} - \hat{\boldsymbol{x}}^n_{k|k-1}),\end{aligned} \tag{27}$$

and

$$\begin{aligned}\boldsymbol{P}^{ll}_{k|k} &= \boldsymbol{P}^{ll}_{k|k-1} - \boldsymbol{K}^{ln}\boldsymbol{S}(\boldsymbol{K}^{ln})^{\mathrm{T}} \\ &= \boldsymbol{P}^{ll}_{k|k-1} - [\boldsymbol{P}^{ln}_{k|k-1}(\boldsymbol{P}^{nn}_{k|k-1})^{-1}\boldsymbol{K}^{nn}]\cdot \\ &\quad \cdot\boldsymbol{S}[\boldsymbol{P}^{ln}_{k|k-1}(\boldsymbol{P}^{nn}_{k|k-1})^{-1}\boldsymbol{K}^{nn}]^{\mathrm{T}} \\ &= \boldsymbol{P}^{ll}_{k|k-1} - \boldsymbol{M}_k[\boldsymbol{K}^{nn}\boldsymbol{S}(\boldsymbol{K}^{nn})^{\mathrm{T}}](\boldsymbol{M}_k)^{\mathrm{T}} \\ &= \boldsymbol{P}^{ll}_{k|k-1} + \boldsymbol{M}_k(\boldsymbol{P}^{nn}_{k|k} - \boldsymbol{P}^{nn}_{k|k-1})(\boldsymbol{M}_k)^{\mathrm{T}},\end{aligned} \tag{28}$$

where $\boldsymbol{M}_k \triangleq \boldsymbol{P}^{ln}_{k|k-1}(\boldsymbol{P}^{nn}_{k|k-1})^{-1}$.

Then, by replacing $\boldsymbol{P}_{k|k}$ and $\boldsymbol{P}_{k|k-1}$ with the integrated form in (8), (23) can be derived as follows,

$$\begin{aligned}\begin{bmatrix}\boldsymbol{P}^{nn}_{k|k} & \boldsymbol{P}^{nl}_{k|k} \\ \boldsymbol{P}^{ln}_{k|k} & \boldsymbol{P}^{ll}_{k|k}\end{bmatrix} &= \begin{bmatrix}\boldsymbol{P}^{nn}_{k|k-1} & \boldsymbol{P}^{nl}_{k|k-1} \\ \boldsymbol{P}^{ln}_{k|k-1} & \boldsymbol{P}^{ll}_{k|k-1}\end{bmatrix} \\ &\quad - \begin{bmatrix}\boldsymbol{K}^{nn}\boldsymbol{S}(\boldsymbol{K}^{nn})^{\mathrm{T}} & \boldsymbol{K}^{nn}\boldsymbol{S}(\boldsymbol{K}^{ln})^{\mathrm{T}} \\ \boldsymbol{K}^{ln}\boldsymbol{S}(\boldsymbol{K}^{nn})^{\mathrm{T}} & \boldsymbol{K}^{ln}\boldsymbol{S}(\boldsymbol{K}^{ln})^{\mathrm{T}}\end{bmatrix},\end{aligned} \tag{29}$$

Hence, the covariances of linear and nonlinear parts for update step are derived as,

$$\begin{aligned}\boldsymbol{P}^{nl}_{k|k} &= \boldsymbol{P}^{nl}_{k|k-1} - \boldsymbol{K}^{nn}\boldsymbol{S}(\boldsymbol{K}^{ln})^{\mathrm{T}} \\ &= \boldsymbol{P}^{nl}_{k|k-1} - \boldsymbol{K}^{nn}\boldsymbol{S}[\boldsymbol{P}^{ln}_{k|k-1}(\boldsymbol{H}^n)^{\mathrm{T}}\boldsymbol{S}^{-1}]^{\mathrm{T}} \\ &= \boldsymbol{P}^{nl}_{k|k-1} - \boldsymbol{K}^{nn}\boldsymbol{S}(\boldsymbol{S}^{-1})^{\mathrm{T}}\boldsymbol{H}^n(\boldsymbol{P}^{ln}_{k|k-1})^{\mathrm{T}} \\ &= \boldsymbol{P}^{nl}_{k|k-1} - \boldsymbol{K}^{nn}\boldsymbol{H}^n\boldsymbol{P}^{nl}_{k|k-1} \\ &= (\boldsymbol{I} - \boldsymbol{K}^{nn}\boldsymbol{H}^n)\boldsymbol{P}^{nl}_{k|k-1} \\ &= \boldsymbol{P}^{nn}_{k|k}(\boldsymbol{P}^{nn}_{k|k-1})^{-1}\boldsymbol{P}^{nl}_{k|k-1} \\ &= \boldsymbol{P}^{nn}_{k|k}(\boldsymbol{M}_k)^{\mathrm{T}},\end{aligned} \tag{30}$$

and

$$\begin{aligned}\boldsymbol{P}^{ln}_{k|k} &= \boldsymbol{P}^{ln}_{k|k-1} - \boldsymbol{K}^{ln}\boldsymbol{S}(\boldsymbol{K}^{nn})^{\mathrm{T}} \\ &= \boldsymbol{P}^{ln}_{k|k-1} - \boldsymbol{P}^{ln}_{k|k-1}(\boldsymbol{H}^n)^{\mathrm{T}}(\boldsymbol{K}^{nn})^{\mathrm{T}} \\ &= \boldsymbol{P}^{ln}_{k|k-1}(\boldsymbol{I} - \boldsymbol{K}^{nn}\boldsymbol{H}^n)^{\mathrm{T}} \\ &= \boldsymbol{P}^{ln}_{k|k-1}[\boldsymbol{P}^{nn}_{k|k}(\boldsymbol{P}^{nn}_{k|k-1})^{-1}]^{\mathrm{T}} \\ &= \boldsymbol{P}^{ln}_{k|k-1}(\boldsymbol{P}^{nn}_{k|k-1})^{-1}\boldsymbol{P}^{nn}_{k|k} \\ &= \boldsymbol{M}_k\boldsymbol{P}^{nn}_{k|k} = (\boldsymbol{P}^{nl}_{k|k})^{\mathrm{T}}.\end{aligned} \tag{31}$$

This completes the proof of Lemma 1. □

Lemma 1 shows that the estimation of linear state variable can be derived from nonlinear one. Hence, we first need to estimate the mean and variance of nonlinear state with SPF algorithm.

Lemma 2: Given the combination structure of linear and nonlinear state variables in (8), the conditional density function $p(\boldsymbol{x}^n_k|\boldsymbol{x}^{n,(i)}_{k-1}, \boldsymbol{x}^l_{k-1})$ for importance sampling of KE-RBPF is

$$p(\boldsymbol{x}^n_k|\boldsymbol{x}^{n,(i)}_{k-1}, \boldsymbol{x}^l_{k-1}) = \mathcal{N}(\bar{\boldsymbol{x}}^{(i)}_{k|k-1}, \boldsymbol{P}^*_{k|k-1}), \tag{32}$$

where

$$\bar{\boldsymbol{x}}^{(i)}_{k|k-1} = \boldsymbol{F}^{nn}\boldsymbol{x}^{n,(i)}_{k-1} + \boldsymbol{F}^{nl}\hat{\boldsymbol{x}}^l_{k-1|k-1}, \tag{33}$$

and

[4] We do not use "≈" because $\boldsymbol{H}$ can be eliminated at last without error.

$$\boldsymbol{P}^{*}_{k|k-1} = \boldsymbol{F}^{nl}\boldsymbol{P}^{ln}_{k-1|k-1}(\boldsymbol{F}^{nn})^{\mathrm{T}} + \boldsymbol{F}^{nn}\boldsymbol{P}^{nl}_{k-1|k-1}(\boldsymbol{F}^{nl})^{\mathrm{T}} + \boldsymbol{F}^{nl}\boldsymbol{P}^{ll}_{k-1|k-1}(\boldsymbol{F}^{nl})^{\mathrm{T}} + \boldsymbol{Q}^{nn}_{k-1}. \quad (34)$$

Proof: Given (8), the mean and variance of nonlinear state are predicted by Kalman filtering algorithm as,

$$\hat{\boldsymbol{x}}^{n}_{k|k-1} = \boldsymbol{F}^{nn}\hat{\boldsymbol{x}}^{n}_{k-1|k-1} + \boldsymbol{F}^{nl}\hat{\boldsymbol{x}}^{l}_{k-1|k-1}, \quad (35)$$

$$\boldsymbol{P}^{nn}_{k|k-1} = \boldsymbol{F}^{nn}\boldsymbol{P}^{nn}_{k-1|k-1}(\boldsymbol{F}^{nn})^{\mathrm{T}} + \boldsymbol{F}^{nl}\boldsymbol{P}^{ln}_{k-1|k-1}(\boldsymbol{F}^{nn})^{\mathrm{T}} + \boldsymbol{F}^{nn}\boldsymbol{P}^{nl}_{k-1|k-1}(\boldsymbol{F}^{nl})^{\mathrm{T}} + \boldsymbol{F}^{nl}\boldsymbol{P}^{ll}_{k-1|k-1}(\boldsymbol{F}^{nl})^{\mathrm{T}} + \boldsymbol{Q}^{nn}_{k-1}, \quad (36)$$

where $\hat{\boldsymbol{x}}^{n}_{k-1|k-1}$ and $\boldsymbol{P}^{nn}_{k-1|k-1}$ are the mean and variance of the previous particle set $\{\boldsymbol{x}^{n,(i)}_{k-1}\}^{N}_{i=1}$. Obviously, to guarantee the consistency in prediction (35) and (36), a correct form of sampling density function (32) should be a Gaussian distribution with mean

$$\bar{\boldsymbol{x}}^{(i)}_{k|k-1} = \boldsymbol{F}^{nn}\boldsymbol{x}^{n,(i)}_{k-1} + \boldsymbol{F}^{nl}\hat{\boldsymbol{x}}^{l}_{k-1|k-1}, \quad (37)$$

and variance

$$\boldsymbol{P}^{*}_{k|k-1} = \boldsymbol{F}^{nl}\boldsymbol{P}^{ln}_{k-1|k-1}(\boldsymbol{F}^{nn})^{\mathrm{T}} + \boldsymbol{F}^{nn}\boldsymbol{P}^{nl}_{k-1|k-1}(\boldsymbol{F}^{nl})^{\mathrm{T}} + \boldsymbol{F}^{nl}\boldsymbol{P}^{ll}_{k-1|k-1}(\boldsymbol{F}^{nl})^{\mathrm{T}} + \boldsymbol{Q}^{nn}_{k-1}. \quad (38)$$

This completes the proof of Lemma 2. □

According to Lemma 2, the new particles are correctly drawn as $\boldsymbol{x}^{n,(i)}_{k} \sim p(\boldsymbol{x}^{n}_{k}|\boldsymbol{x}^{n,(i)}_{k-1}, \boldsymbol{x}^{l}_{k-1})$. The mean and variance of nonlinear state in the prediction step can be calculated with the previous weight set $\{w^{(i)}_{k-1}\}^{N}_{i=1}$ of particles as

$$\hat{\boldsymbol{x}}^{n}_{k|k-1} = \sum_{i=1}^{N} w^{(i)}_{k-1}\boldsymbol{x}^{n,(i)}_{k}, \quad (39)$$

$$\boldsymbol{P}^{nn}_{k|k-1} = \sum_{i=1}^{N} w^{(i)}_{k-1}(\boldsymbol{x}^{n,(i)}_{k} - \hat{\boldsymbol{x}}^{n}_{k|k-1})(\boldsymbol{x}^{n,(i)}_{k} - \hat{\boldsymbol{x}}^{n}_{k|k-1})^{\mathrm{T}}, \quad (40)$$

where N is the amount of particles. Then, the weights of particles are updated by the standard PF algorithm as $w^{(i)}_{k-1} \rightarrow w^{(i)}_{k}$. The mean $\hat{\boldsymbol{x}}^{n}_{k|k}$ and variance $\boldsymbol{P}^{nn}_{k|k}$ of nonlinear state in the update step are calculated from (39) and (40) by replacing $w^{(i)}_{k-1}$ with $w^{(i)}_{k}$.

Finally, the estimation of linear part of target state can be derived from the correlation between $\boldsymbol{x}^{n}_{k}$ and $\boldsymbol{x}^{l}_{k}$ in Lemma 1. The summary of the our KE-RBPF algorithm is provided in Algorithm 2.

Algorithm 2 KE-RBPF for Radar Tracking

Input: $N \in \mathbb{N}_{+}$, the prior probability p_0 of $\boldsymbol{x}^{n}$, the mean $\bar{\boldsymbol{x}}^{l}_{0}$ and variance $\bar{\boldsymbol{P}}^{ll}_{0}$ of $\boldsymbol{x}^{l}$, and the tracking model (1).

Output: particles $\{\boldsymbol{x}^{n,(i)}_{k}\}^{N}_{i=1}$ and weights $\{w^{(i)}_{k}\}^{N}_{i=1}$ of nonlinear part. Estimation mean $\hat{\boldsymbol{x}}^{l}_{k|k}$ and variance $\boldsymbol{P}^{ll}_{k|k}$ of linear part, at time step k.

Initialize: for $i = 1, 2, ..., N$, draw particle $\boldsymbol{x}^{n,(i)}_{0} \sim p_0$ and calculate weight $w^{(i)}_{0} = 1/N$. $\hat{\boldsymbol{x}}^{l}_{0|0} = \bar{\boldsymbol{x}}^{l}_{0}$, $\boldsymbol{P}^{ll}_{0|0} = \bar{\boldsymbol{P}}^{ll}_{0}$

For: time step $k = 1, 2, 3....$

1: New particle $\boldsymbol{x}^{n,(i)}_{k}$ is drawn from $p(\boldsymbol{x}^{n}_{k}|\boldsymbol{x}^{n,(i)}_{k-1}, \boldsymbol{x}^{l}_{k-1})$ with (32) for nonlinear state prediction, where $i = 1, ..., N$.
2: Mean $\hat{\boldsymbol{x}}^{n}_{k|k-1}$ and variance $\boldsymbol{P}^{nn}_{k|k-1}$ in nonlinear prediction are calculated with particle set $\{\boldsymbol{x}^{n,(i)}_{k}\}^{N}_{i=1}$ and previous weight set $\{w^{(i)}_{k-1}\}^{N}_{i=1}$ in (39) and (40).
3: $\hat{\boldsymbol{x}}^{l}_{k|k-1}$, $\boldsymbol{P}^{ll}_{k|k-1}$ and $\boldsymbol{P}^{ln}_{k|k-1}$ are calculated with (14), (15) and (16) for linear state prediction.
4: $w^{(i)}_{k}$ is updated as $w^{(i)}_{k} = \frac{p(\boldsymbol{z}_k|\boldsymbol{x}^{n,(i)}_{k|k-1})}{C_k} w^{(i)}_{k-1}$, given observation $\boldsymbol{z}_k$, , where C_k is the normalized constant and $i = 1, ..., N$.
5: Particle resampling (optional).
6: Mean $\hat{\boldsymbol{x}}^{n}_{k|k}$ and variance $\boldsymbol{P}^{n}_{k|k}$ in nonlinear update are calculated with new weight set $\{w^{(i)}_{k}\}^{N}_{i=1}$.
7: $\hat{\boldsymbol{x}}^{l}_{k|k}$, $\boldsymbol{P}^{ll}_{k|k}$ and $\boldsymbol{P}^{ln}_{k|k}$ are calculated with (18), (19) and (20) for linear state update.

End

IV. SIMULATION RESULTS

In this section, we concentrate on a two-dimensional (2-D) tracking problem. To validate the effectiveness of our KE-RBPF algorithm, a radar system without the observation information on velocity is utilized to track the target. In addition, the observation noise is set to be glint noise. This noise is a classic non-Gaussian noise which exists commonly in the radar observation process when target glints [28]. Moreover, we select one constant-velocity (CV) and two constant-turn (CT) kinematic models to simulate the target trajectories with Cartesian coordinate. For each target trajectory, 100 Monte Carlo (MC) simulations are run. In each run, the root-mean-square-error (RMSE) of tracking results is evaluated. Then, the statistical results of the RMSE in 100 MC runs are provided to validate the effectiveness of our KE-RBPF algorithm, in comparison with other algorithms including SPF [7], UPF [9] and RBPF [11].[5] The statistical results contain mean, deviation and CTE, which are estimated by the latest method called iterative mid-range (IMR) [25].

A. SIMULATION SETUP

In the conventional 2-D radar tracking problem, the original SS model is shown in the following:

$$\textbf{Transition equation}: \ \boldsymbol{x}_k = \boldsymbol{F}\boldsymbol{x}_{k-1} + \boldsymbol{v}_{k-1} \quad (41a)$$

$$\textbf{Observation equation}: \ \boldsymbol{z}_k = \boldsymbol{h}(\boldsymbol{x}_k) + \boldsymbol{w}_k, \quad (41b)$$

where $\boldsymbol{x}_k = [d_{x,k}, \ d_{y,k}, \ v_{x,k}, \ v_{y,k}]^{\mathrm{T}}$ is the tracking state vector, indicating the 2-D distance $[d_{x,k}, \ d_{y,k}]^{\mathrm{T}}$ and velocity $[v_{x,k}, \ v_{y,k}]^{\mathrm{T}}$ in the $x - y$ plane at time step k.

[5] It is called MPF algorithm in that paper

$\boldsymbol{F}$ is the state transition matrix with sampling interval s_τ, which produces the CV and CT trajectories with two different models, according to the tracking theory for cruising and maneuvering targets [23]. In our simulation, we have

$$\boldsymbol{F} = \begin{bmatrix} 1 & 0 & s_\tau & 0 \\ 0 & 1 & 0 & s_\tau \\ 0 & 0 & 1 & 0 \\ 0 & 0 & 0 & 1 \end{bmatrix} \tag{42}$$

for CV trajectory. In addition, we have

$$\boldsymbol{F} = \begin{bmatrix} 1 & 0 & \frac{\sin(\alpha s_\tau)}{\alpha} & \frac{\cos(\alpha s_\tau)-1}{\alpha} \\ 0 & 1 & \frac{1-\cos(\alpha s_\tau)}{\alpha} & \frac{\sin(\alpha s_\tau)}{\alpha} \\ 0 & 0 & \cos(\alpha s_\tau) & -\sin(\alpha s_\tau) \\ 0 & 0 & \sin(\alpha s_\tau) & \cos(\alpha s_\tau) \end{bmatrix}, \tag{43}$$

for CT trajectories with known turn rates $\alpha = 2.5°/s$ and $\alpha = 5°/s$ [29]. $\boldsymbol{v}_{k-1} = [v_d, \ v_d, \ v_v, \ v_v]^{\mathrm{T}}$ represents the state transition noise in distance and velocity, which obeys the Gaussian distribution, i.e., $v_d \sim \mathcal{N}(v_d; 0, \sigma_d^2)$ and $v_v \sim \mathcal{N}(v_v; 0, \sigma_v^2)$. Here, σ_d and $\sigma_v = 2\sigma_d/s_\tau$ are standard deviations of transition noise of distance and velocity, respectively. The three trajectories are plotted in Figure 2.

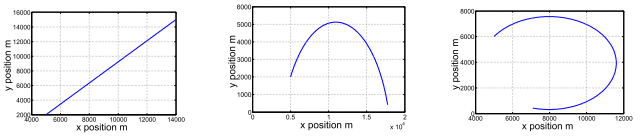

FIGURE 2. Three trajectories of target. (a) trajectory of CV model. (b) trajectory of CT model (turn rate $\alpha = 2.5°/s$). (c) trajectory of CT model (turn rate $\alpha = 5°/s$).

In addition, the radar system without observation on velocity is used for tracking, which uses the spherical coordinate to track target and only contains the observation on distance and azimuth. Specifically, the nonlinear observation equation of (41b) is re-defined to be the following nonlinear function:

$$\underbrace{\begin{bmatrix} \theta_k \\ r_k \end{bmatrix}}_{\boldsymbol{z}_k} = \begin{bmatrix} \arctan \dfrac{d_{y,k}}{d_{x,k}} \\ \sqrt{d_{x,k}^2 + d_{y,k}^2} \end{bmatrix} + \underbrace{\begin{bmatrix} w_\theta \\ w_r \end{bmatrix}}_{\boldsymbol{w}}, \tag{44}$$

where $\boldsymbol{z}_k = [\theta_k, \ r_k]^{\mathrm{T}}$ denotes the observation vector with azimuth θ_k and distance r_k, at time k, respectively. In (44), $\boldsymbol{w} = [w_\theta, \ w_r]^{\mathrm{T}}$ is the glint noise of observation vector containing azimuth and distance parts, i.e., w_θ and w_r.

Obviously, from (1c) and (44), the nonlinear part of tracking state is $\boldsymbol{x}_k^n = [d_{x,k}, \ d_{y,k}]^{\mathrm{T}}$ with noise $\boldsymbol{v}_k^n = [v_d, \ v_d]^{\mathrm{T}}$, and the linear part is $\boldsymbol{x}_k^l = [v_{x,k}, \ v_{y,k}]^{\mathrm{T}}$ with noise $\boldsymbol{v}_k^l = [v_v, \ v_v]^{\mathrm{T}}$. Furthermore, according to (51) and (43), the transition matrices of (1) for CV trajectory are defined as

$$\boldsymbol{F}^{nn} = \begin{bmatrix} 1 & 0 \\ 0 & 1 \end{bmatrix} \boldsymbol{F}^{nl} = \begin{bmatrix} s_\tau & 0 \\ 0 & s_\tau \end{bmatrix}$$

$$\boldsymbol{F}^{ln} = \begin{bmatrix} 0 & 0 \\ 0 & 0 \end{bmatrix} \boldsymbol{F}^{ll} = \begin{bmatrix} 1 & 0 \\ 0 & 1 \end{bmatrix}, \tag{45}$$

and transition matrices of (1) for CT trajectory are defined as

$$\boldsymbol{F}^{nn} = \begin{bmatrix} 1 & 0 \\ 0 & 1 \end{bmatrix} \boldsymbol{F}^{nl} = \begin{bmatrix} \frac{\sin(\alpha s_\tau)}{\alpha} & \frac{\cos(\alpha s_\tau)-1}{\alpha} \\ \frac{1-\cos(\alpha s_\tau)}{\alpha} & \frac{\sin(\alpha s_\tau)}{\alpha} \end{bmatrix}$$

$$\boldsymbol{F}^{ln} = \begin{bmatrix} 0 & 0 \\ 0 & 0 \end{bmatrix} \boldsymbol{F}^{ll} = \begin{bmatrix} \cos(\alpha s_\tau) & -\sin(\alpha s_\tau) \\ \sin(\alpha s_\tau) & \cos(\alpha s_\tau) \end{bmatrix}. \tag{46}$$

As mentioned before, the observation noise is defined as the glint noise, which can be modeled as a mixture of a Gaussian noise with high probability and moderate variance and a (heavy-tailed) Laplacian distributed noise with low probability [30], i.e.,

$$p(\boldsymbol{w}) = (1-\epsilon) \cdot p_G(\boldsymbol{w}) + \epsilon \cdot p_L(\boldsymbol{w}), \tag{47}$$

where ϵ is the glint probability. In (47), the subscripts G and L stand for Gaussian and Laplacian, respectively, i.e.,

$$p_G(\boldsymbol{w}) \triangleq \frac{1}{\sqrt{2\pi}\boldsymbol{\sigma}_G} e^{-(\boldsymbol{w}-\hat{\boldsymbol{w}}_G)^2/2\sigma_G^2}, \tag{48}$$

$$p_L(\boldsymbol{w}) \triangleq \frac{1}{2\boldsymbol{\sigma}_L} e^{-|\boldsymbol{w}-\hat{\boldsymbol{w}}_L|/\boldsymbol{\sigma}_L}, \tag{49}$$

where $\hat{\boldsymbol{w}}_G$ and $\boldsymbol{\sigma}_G$ are the mean and deviation for Gaussian distribution, and $\hat{\boldsymbol{w}}_L$ and $\boldsymbol{\sigma}_L$ are the mean and deviation for Laplacian distribution. In our tracking model, the observation noise w_θ and w_r are independent. Hence, we have

$$p(\boldsymbol{w}) = (1-\epsilon)p_{G,\theta}(w_\theta)p_{G,r}(w_r) + \epsilon p_{L,\theta}(w_\theta)p_{L,r}(w_r), \tag{50}$$

where $p_{G,\theta}(w_\theta)$ and $p_{L,\theta}(w_\theta)$ are the Gaussian and Laplacian distributions of azimuth with means $\hat{w}_{G,\theta}$ and $\hat{w}_{L,\theta}$ and deviations $\sigma_{G,\theta}$ and $\sigma_{L,\theta}$, respectively. In (50), $p_{G,r}(w_r)$ and $p_{L,r}(w_r)$ are the Gaussian and Laplacian distributions of distance with means $\hat{w}_{G,r}$ and $\hat{w}_{L,r}$ and deviations $\sigma_{G,r}$ and $\sigma_{L,r}$, respectively. ϵ is set to be 0.2, according to the conventional glint noise model in [30].

B. EVALUATION

In our simulation, according to [30], the target tracking scenario for each trajectory is simulated with the parameters set in Table 2. Beside, the initial state for target tracking is set as $\boldsymbol{x}_0 = [5km, \ 2km, \ 0.18km/s, \ 0.26km/s]^{\mathrm{T}}$. Beginning with $\boldsymbol{x}_0$, our trajectories are simulated with the transition equation of (41a), given different kinematic models of (51) and (43). The simulation time is set to be $30s$. Then, these trajectories are observed by the conventional radar system (41b) with glint noise. The distribution of glint noise is computed with (47). Furthermore, our KE-RBPF and other algorithms are used to track the target according to the observations, and the tracking RMSE of azimuth and distance is obtained. Finally, Figures 3 to 8 show the statistical results of our and other algorithms over 100 MC runs, in terms of means, deviations and CTE for different trajectories.

TABLE 2. Parameters Setting.

Parameters	Setting
s_τ	0.1 s
α	2.5 or 5 $^\circ/s$
σ_d	10 m
$\hat{w}_{G,\theta}$ and $\hat{w}_{L,\theta}$	0 rad
$\hat{w}_{G,r}$ and $\hat{w}_{L,r}$	0 m
$\sigma_{G,\theta}$	0.001 rad
$\sigma_{L,\theta}$	0.01 rad
$\sigma_{G,r}$	2 m
$\sigma_{L,r}$	20 m
ϵ	0.2
The number of particle	100

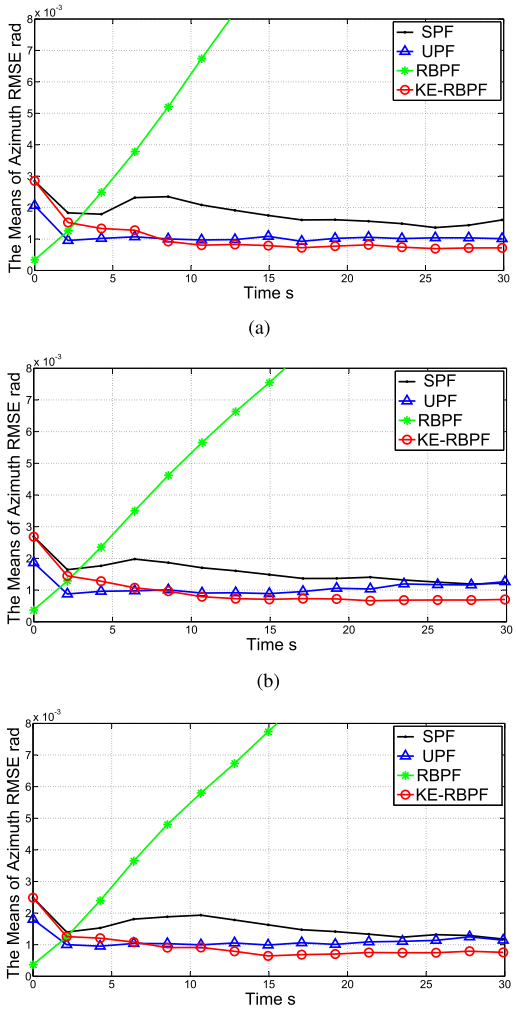

FIGURE 3. Means of tracking RMSE on azimuth for different trajectories. (a) CV trajectory. (b) CT trajectory with $\alpha = 2.5°/s$. (c) CT trajectory with $\alpha = 5°/s$.

1) MEANS OF TRACKING RMSE FOR DIFFERENT TRAJECTORIES

The means of tracking RMSE on azimuth and distance for CV and CT trajectories are shown in Figures 3 and 4, respectively. Obviously, we can see from these figures that the

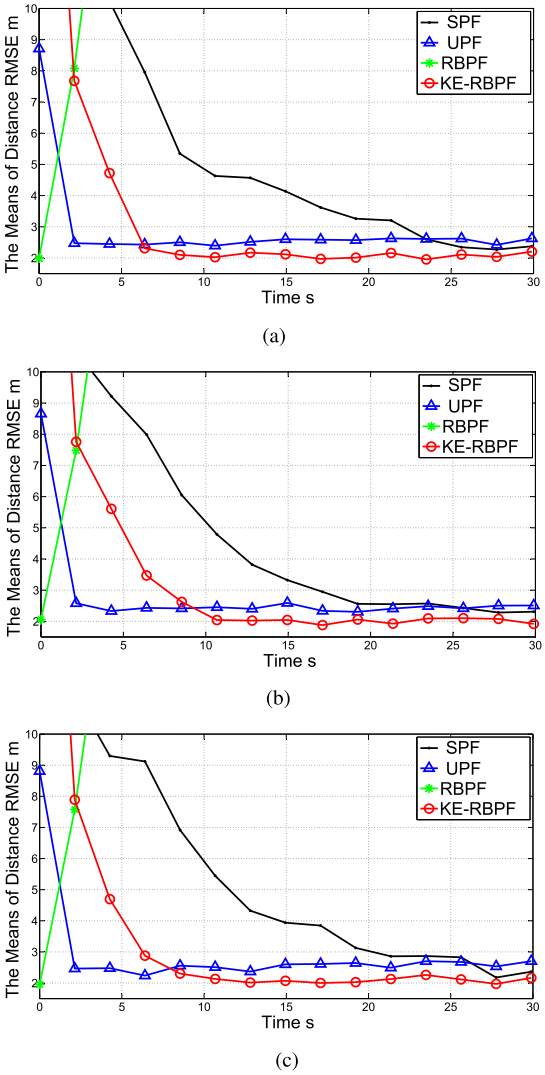

FIGURE 4. Means of tracking RMSE on distance for different trajectories. (a) CV trajectory. (b) CT trajectory with $\alpha = 2.5°/s$. (c) CT trajectory with $\alpha = 5°/s$.

means of tracking RMSE on RBPF increase much faster than other algorithms. This degradation of RBPF in tracking performance verifies that the RBPF algorithm does not fit for conventional radar tracking system of (41b), as the observation information on the linear part of target state is missing. Among the remaining three algorithms, the means of tracking RMSE of our KE-RBPF algorithm is the smallest after 10 seconds. Specifically, the average means of RMSE after 10 seconds of our and other algorithms are shown in Tables 3 and 4. In these two tables, we can see that the average means of RMSE of our KE-RBPF for azimuth tracking decrease around 50% and 25%, in comparison with SPF and UPF algorithms. Besides, for distance tracking, average means of our KE-RBPF decrease around 37% and 19%, in comparison with SPF and UPF algorithms. It can be thus concluded that our KE-RBPF algorithm produces the best tracking trajectories.

TABLE 3. Average means of tracking RMSE for azimuth after 10 Second.

	CV trajectory	CT trajectory with $\alpha = 2.5°/s$	CT trajectory with $\alpha = 5°/s$
SPF	1.64 mrad	1.39 mrad	1.46 mrad
UPF	1.01 mrad	1.05 mrad	1.08 mrad
KE-RBPF	0.76 mrad	0.71 mrad	0.75 mrad

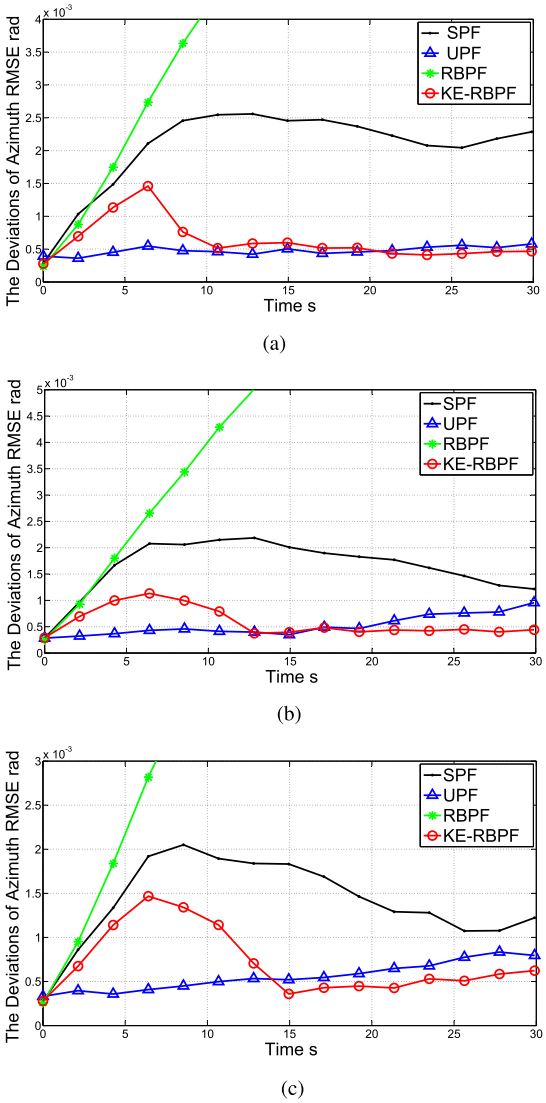

FIGURE 5. Deviations of tracking RMSE on azimuth for different trajectories. (a) CV trajectory. (B) CT trajectory with $\alpha = 2.5°/s$. (C) CT trajectory with $\alpha = 5°/s$.

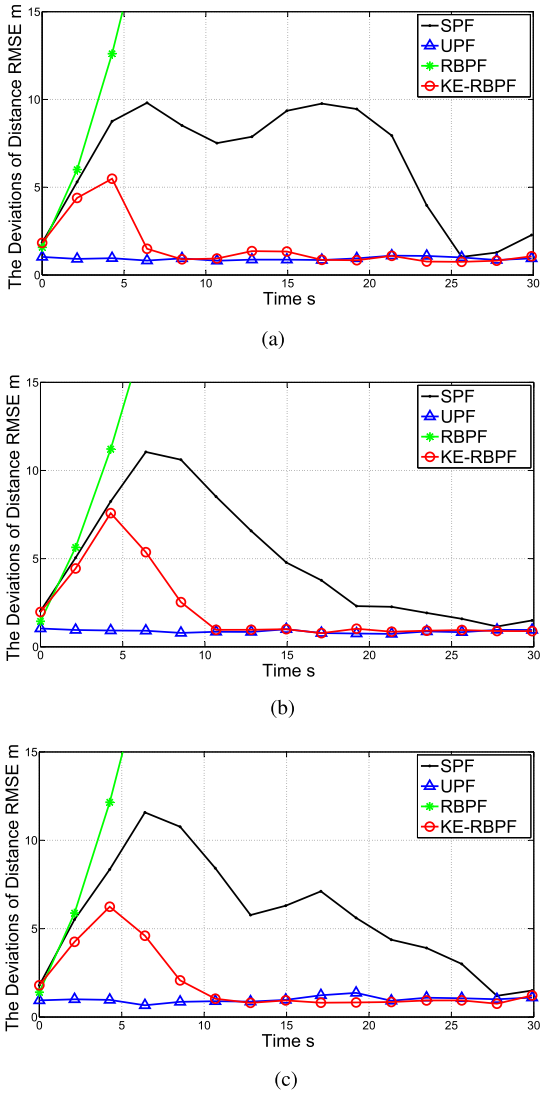

FIGURE 6. Deviations of tracking RMSE on distance for different trajectories. (a) CV trajectory. (b) CT trajectory with $\alpha = 2.5°/s$. (c) CT trajectory with $\alpha = 5°/s$.

2) DEVIATIONS OF TRACKING RMSE FOR DIFFERENT TRAJECTORIES

The deviations of tracking RMSE on azimuth and distance for CV and CT trajectories are shown in Figures 5 and 6. From these figures, the performance of RBPF degrades very fast as expected. In addition, the SPF cannot perform well in comparison with UPF and our KE-RBPF. Although the deviations of our KE-RBPF are larger than UPF algorithm before 15 second, they sharply decrease along with time, and keep a similar level to UPF after 15 seconds. Specifically, the average deviations of RMSE after 15 seconds of three algorithms, i.e., SPF, UPF and KE-RBPF, are shown in Tables 5 and 6. In these two tables, we can see that the deviations of our KE-RBPF and UPF algorithms are similar and they are much smaller than those of SPF. Therefore, both our KE-RBPF and UPF outperform the SPF on tracking stability.

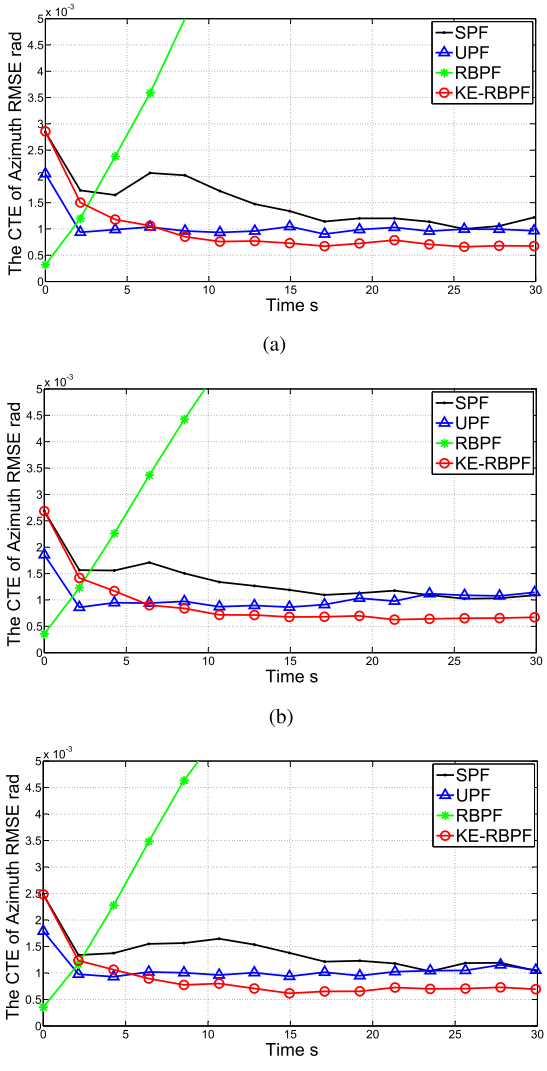

FIGURE 7. CTE of tracking RMSE on azimuth for different trajectories. (a) CV trajectory. (b) CT trajectory with $\alpha = 2.5°/s$. (c) CT trajectory with $\alpha = 5°/s$.

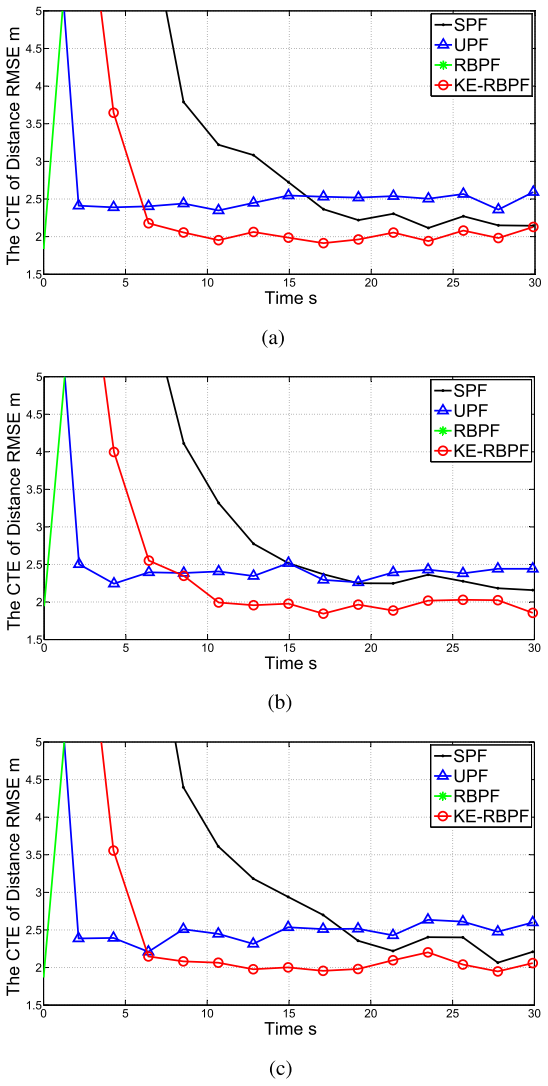

FIGURE 8. CTE of tracking RMSE on distance for different trajectories. (a) CV trajectory. (b) CT trajectory with $\alpha = 2.5°/s$. (c) CT trajectory with $\alpha = 5°/s$.

3) CTE OF TRACKING RMSE FOR DIFFERENT TRAJECTORIES

The CTE of tracking RMSE in 100 MC runs is investigated, and the results are shown in Figures 7 and 8, respectively. Obviously, the performance of RBPF still degrades much fast. In the rest of three algorithms, our KE-RBPF outperforms others after around 6 seconds. As of the discussed in [24], the CTE reflects what the large majority of the data are about and its measures are usually construed as representatives of the data set. Hence, our KE-RBPF produces the best tracking performance in comparison with other algorithms. Specifically, the average CTE of SPF, UPF and KE-RBPF algorithms after 6 seconds are shown in Tables 7 and 8, further validating the effectiveness of our KE-RBPF algorithm.

4) DISCUSSION ON THE KE-RBPF PERFORMANCE WITH DIFFERENT ϵ

To investigate the relationship between the value of ϵ and the performance of our method, we conduct a tracking simulation, in which different ϵ is set to produce different glint noises. The tracking model is constant turn (CT) model with turn rate $\alpha = 2.5°/s$. For each ϵ, 100 MC simulations are run with 30 s tracking time. The tracking performance, in terms of means, deviations and CTE of tracking RMSE for azimuth and distance, is reported in Table 9. In this table, we can see that the performance of our KE-RBPF becomes better when the value of ϵ decreases. In this paper, we set up our simulation with $\epsilon = 0.2$ for keeping consistency with the previous works [30] in the practical application, but it performs better with smaller ϵ.

5) SIMULATION ON TRACKING WITH 6 DIMENSIONAL SS MODEL

In this subsection, we extend the SS model to 6 dimension, containing three-dimensional-Cartesian-coordinate values and the corresponding velocities. Accordingly, we set the

TABLE 4. Average means of tracking RMSE for distance after 10 second.

	CV trajectory	CT trajectory with $\alpha = 2.5°/s$	CT trajectory with $\alpha = 5°/s$
SPF	3.30 m	2.96 m	3.38 m
UPF	2.56 m	2.44 m	2.48 m
KE-RBPF	2.08 m	2.02 m	2.09 m

TABLE 5. Average deviations of tracking RMSE for azimuth after 15 second.

	CV trajectory	CT trajectory with $\alpha = 2.5°/s$	CT trajectory with $\alpha = 5°/s$
SPF	2.32 mrad	1.74 mrad	1.47 mrad
UPF	0.49 mrad	0.60 mrad	0.64 mrad
KE-RBPF	0.49 mrad	0.46 mrad	0.58 mrad

TABLE 6. Average deviations of tracking RMSE for distance after 15 second.

	CV trajectory	CT trajectory with $\alpha = 2.5°/s$	CT trajectory with $\alpha = 5°/s$
SPF	6.05 m	3.44 m	4.72 m
UPF	0.93 m	0.86 m	1.05 m
KE-RBPF	0.98 m	0.92 m	0.91 m

TABLE 7. Average CTE of tracking RMSE for azimuth after 6 second.

	CV trajectory	CT trajectory with $\alpha = 2.5°/s$	CT trajectory with $\alpha = 5°/s$
SPF	1.38 mrad	1.22 mrad	1.31 mrad
UPF	0.98 mrad	0.99 mrad	1.01 mrad
KE-RBPF	0.76 mrad	0.71 mrad	0.72 mrad

TABLE 8. Average CTE of tracking RMSE for distance after 6 second.

	CV trajectory	CT trajectory with $\alpha = 2.5°/s$	CT trajectory with $\alpha = 5°/s$
SPF	2.88 m	2.88 m	3.13 m
UPF	2.48 m	2.39 m	2.48 m
KE-RBPF	2.02 m	2.04 m	2.05 m

TABLE 9. Average tracking performance over the whole tracking time with all MC runs, in comparison with different values of ϵ.

	$\epsilon = 0.05$	$\epsilon = 0.1$	$\epsilon = 0.2$	$\epsilon = 0.3$
mean for azimuth(mrad)	0.38	0.49	0.71	1.01
mean for distance(m)	1.01	1.32	2.02	2.96
deviation for azimuth(mrad)	0.19	0.23	0.46	0.77
deviations for distance(m)	0.37	0.43	0.92	1.64
CTE for azimuth(mrad)	0.38	0.48	0.71	0.99
CTE for distance(m)	1.08	1.31	2.04	2.80

target state $\boldsymbol{x}_k$ in (41a) as $\boldsymbol{x}_k = [d_{x,k},\ d_{y,k},\ d_{z,k}\ v_{x,k},\ v_{y,k},\ v_{z,k}]^{\mathrm{T}}$. It contains three dimensional distance $[d_{x,k},\ d_{y,k},\ d_{z,k}]^{\mathrm{T}}$ and velocity $[v_{x,k},\ v_{y,k},\ v_{z,k}]^{\mathrm{T}}$ in the $x-y-z$ space at time step k. The transition matrix is set to be

$$\boldsymbol{F} = \begin{bmatrix} 1 & 0 & 0 & s_\tau & 0 & 0 \\ 0 & 1 & 0 & 0 & s_\tau & 0 \\ 0 & 0 & 1 & 0 & 0 & s_\tau \\ 0 & 0 & 0 & 1 & 0 & 0 \\ 0 & 0 & 0 & 0 & 1 & 0 \\ 0 & 0 & 0 & 0 & 0 & 1 \end{bmatrix} \tag{51}$$

In (41a), $\boldsymbol{v}_{k-1}$ denotes the six dimensional state transition noise in distance and velocity, i.e., $\boldsymbol{v}_{k-1} = [v_d,\ v_d,\ v_d,\ v_v,\ v_v,\ v_v]^{\mathrm{T}}$. In addition, the observation equation of (41b) is re-defined to be a three-dimensional-spherical-coordinate equation as follows,

$$\underbrace{\begin{bmatrix} \theta_k \\ r_k \\ \beta_k \end{bmatrix}}_{\boldsymbol{z}_k} = \begin{bmatrix} \arctan \dfrac{d_{y,k}}{d_{x,k}} \\ \sqrt{d_{x,k}^2 + d_{y,k}^2} \\ \arctan \dfrac{d_{z,k}}{\sqrt{d_{x,k}^2 + d_{y,k}^2}} \end{bmatrix} + \underbrace{\begin{bmatrix} w_\theta \\ w_r \\ w_\beta \end{bmatrix}}_{\boldsymbol{w}}, \tag{52}$$

where β_k denotes the parameter of pitch in target state with observation glint noise w_β. All parameters are set in Table 2.

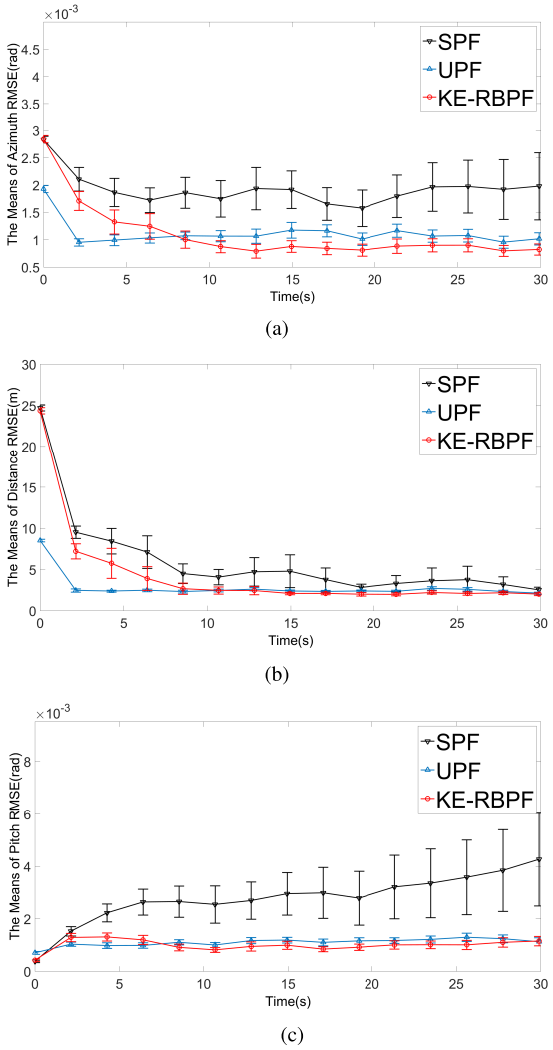

FIGURE 9. Means of tracking RMSE on azimuth, distance and pitch with error bars of 1/5 deviations. (a) Azimuth Tracking Performance. (b) Distance Tracking Performance. (c) Pitch Tracking Performance.

In the aforementioned tracking scenario, we test our KE-RBPF to track a target with constant velocity model in the three dimensional space, comparing to SPF and UPF algorithms. We simulate this tracking procedure over 100 MC runs. The tracking performance on the means is shown in Figure 9, with the error bars of 1/5 deviations. From this figure, we can see that our KE-RBPF yields the smallest means of tracking RMSE in azimuth, distance and pitch, in comparison with PF and UPF algorithms. Moreover, our KE-RBPF yields the same deviation as the UPF algorithm, which is better than SPF.

6) DISCUSSION ON COMPUTATIONAL COMPLEXITY

In the aforementioned statistical results, our KE-RBPF produces the best performance on means and CTE, and UPF performs best on deviations. Although the tracking performance of UPF on deviation is best, the computational time of UPF limits its application in real condition. In fact, because of the extra computation of unscented Kalman filtering for each particle at each time step [9], the time consumption of UPF algorithm is lager than our KE-RBPF. To further discuss the computational complexity, we have recorded the computational time of one iteration in the simulation for all aforementioned algorithms. Specially, the computer used for the test is with Intel Core i7-3770 CPU at 3.4 GHz and 4 GB RAM. In our conventional radar tracking scenario, the computational time of each iteration for all algorithms is listed as: a) SPF, 28.4(ms); b) UPF, 87.5(ms); c) RBPF, 24.0(ms); d) KE-RBPF, 26.6(ms). Obviously, our KE-RBPF is as fast as RBPF, and much faster than UPF which ranks the best in tracking performance in terms of deviation among all compared algorithms. In summary, our KE-RBPF algorithm outperforms the other classic algorithms in nonlinear and non-Gaussian radar tracking scenarios, and its computational time is small as well. Since it is intractable to obtain the field data in radar tracking, we follow [23] to set up our simulation scenario, which is also the benchmark for radar tracking simulation [1], [31]–[34].

V. CONCLUSIONS

In this paper, we have proposed a novel KE-RBPF algorithm to track target with linear/nonlinear SS model. First, in the conventional radar tracking scenarios, a gradual deviation problem about tracking by original RBPF algorithm was discussed. Then, a novel KE-RBPF algorithm was proposed in light of the Kalman estimation framework. Based on this framework, a new formulation on the correlation between linear and nonlinear parts of target state was investigated. Benefiting from this correlation, we solved the deviation problem by correctly updating the linear part with the information from nonlinear. Finally, the simulations verified that our KE-RBPF algorithm improves the tracking performance on nonlinear and non-Gaussian tracking scenarios.

There are three directions of the future works in our paper. (1) In fact, our KE-RBPF utilizes the second order statistic information (variances) of nonlinear part of target state to update the linear part, by which we obtain a better tracking performance than original RBPF. Hence, a higher order statistic information can be considered in the future to further reduce the tracking error. (2) Our KE-RBPF estimates the target state in the form of means and variances, which can also be used as the tracking algorithm of sensor node for distributed fusion network. This can be seen as a promising future work. (3) Our KE-RBPF algorithm cannot obtain a good tracking performance at the initial stage. Some preprocessing methods may be combined with our KE-RBPF for further improving the initial performance of our algorithm.

ACKNOWLDGEMENT

This paper was presented at WCSP 2016 [1].

REFERENCES

[1] J. Liu, Z. Wang, and M. Xu, "A nonlinear and non-Gaussian distributed fusion based on Rao–Blackwellized particle filtering," in *Proc. 8th Int. Conf. Wireless Commun. Signal Process. (WCSP)*, Oct. 2016, pp. 1–5.
[2] M. S. Arulampalam, S. Maskell, N. Gordon, and T. Clapp, "A tutorial on particle filters for online nonlinear/non-Gaussian Bayesian tracking," *IEEE Trans. Signal Process.*, vol. 50, no. 2, pp. 174–188, Feb. 2002.
[3] J. Liu, Z. Wang, and M. Xu, "A novel distributed fusion algorithm for multi-sensor nonlinear tracking," *EURASIP J. Adv. Signal Process*, vol. 2016, no. 1, pp. 1–11, 2016. [Online]. Available: http://dx.doi.org/10.1186/s13634-016-0362-y
[4] Y. Bar-Shalom, X. Li, and T. Kirubarajan, *Estimation With Applications to Tracking and Navigation: Theory Algorithms and Software*. Hoboken, NJ, USA: Wiley, 2004.
[5] R. E. Kalman, "A new approach to linear filtering and prediction problems," *Trans. ASME, D, J. Basic Eng.*, vol. 82, pp. 35–45, Sep. 1960.
[6] S. Julier, J. Uhlmann, and H. F. Durrant-Whyte, "A new method for the nonlinear transformation of means and covariances in filters and estimators," *IEEE Trans. Autom. Control*, vol. 45, no. 3, pp. 477–482, Mar. 2000.
[7] A. Doucet and A. Johansen, "A tutorial on particle filtering and smoothing: Fifteen years later," *Handbook Nonlinear Filtering*, vol. 12, nos. 656–704, pp. 1–3, 2009.
[8] A. Doucet and X. Wang, "Monte Carlo methods for signal processing: A review in the statistical signal processing context," *IEEE Signal Process. Mag.*, vol. 22, no. 6, pp. 152–170, Nov. 2005.
[9] R. Van Der Merwe, A. Doucet, N. De Freitas, and E. Wan, "The unscented particle filter," in *Proc. NIPS*, 2000, pp. 584–590.
[10] A. Doucet, S. Godsill, and C. Andrieu, "On sequential Monte Carlo sampling methods for Bayesian filteringz," *Statist. Comput.*, vol. 10, no. 3, pp. 197–208, 2000.
[11] T. Schön, F. Gustafsson, and P. Nordlund, "Marginalized particle filters for mixed linear/nonlinear state-space models," *IEEE Trans. Signal Process.*, vol. 53, no. 7, pp. 2279–2289, Sep. 2005.
[12] C. Andrieu and A. Doucet, "Particle filtering for partially observed Gaussian state space models," *J. Roy. Statist. Soc. B Statist. Methodol.*, vol. 64, no. 4, pp. 827–836, Oct. 2002.
[13] F. Lindsten and T. Schön, and J. Olsson, "An explicit variance reduction expression for the Rao–Blackwellised particle filter," *Control Eng.*, vol. 44, no. 1, pp. 11979–11984, 2011.
[14] C. Wen, L. Qin, Q. Zhu, C. Wang, and J. Li, "Three-dimensional indoor mobile mapping with fusion of two-dimensional laser scanner and RGB-D camera data," *IEEE Geosci. Remote Sens. Lett.*, vol. 11, no. 4, pp. 843–847, Apr. 2014.
[15] J. Kim, Z. Lin, and I. Kweon, "Rao–Blackwellized particle filtering with Gaussian mixture models for robust visual tracking," *Comput. Vis. Image Understand.*, vol. 125, pp. 128–137, Sep. 2014.
[16] E. Baziw, "Real-time seismic signal enhancement utilizing a hybrid Rao–Blackwellized particle filter and hidden Markov model filter," *IEEE Geosci. Remote Sens. Lett.*, vol. 2, no. 4, pp. 418–422, Oct. 2005.
[17] E. Özkan, F. Lindsten, C. Fritsche, and F. Gustafsson, "Recursive maximum likelihood identification of jump Markov nonlinear systems," *IEEE Trans. Signal Process.*, vol. 63, no. 3, pp. 754–765, Feb. 2015.
[18] Z. S. Zhao *et al.*, "Improved Rao–Blackwellized particle filter by particle swarm optimization," *J. Appl. Math.*, vol. 2013, no. 2, pp. 1–7, 2013.
[19] Y. Han, "A Rao–Blackwellized particle filter for adaptive beamforming with strong interference," *IEEE Trans. Signal Process.*, vol. 60, no. 60, pp. 2952–2961, Sep. 2012.
[20] K. Berntorp, A. Robertsson, and K. E. Arzen, "Rao–Blackwellized particle filters with out-of-sequence measurement processing," *IEEE Trans. Signal Process.*, vol. 62, no. 24, pp. 6454–6467, Sep. 2014.
[21] G. Hendeby, R. Karlsson, and F. Gustafsson, "The Rao–Blackwellized particle filter: A filter bank implementation," *EURASIP J. Adv. Signal Process*, vol. 2010, no. 1, pp. 1–10, 2010.
[22] H. You, X. Jianjuan, and G. Xin, *Radar Data Processing With Applications*. Hoboken, NJ, USA: Wiley, 2016.
[23] X. R. Li and V. P. Jilkov, "Survey of maneuvering target tracking. Part I. Dynamic models," *IEEE Trans. Aerosp. Electron. Syst.*, vol. 39, no. 4, pp. 1333–1364, Oct. 2003.
[24] H. Yin, J. Lan, and X. Li, "New robust metrics of central tendency for estimation performance evaluation," in *Proc. IEEE 15th Int. Conf. Inf. Fusion (FUSION)*, Jun. 2012, pp. 2020–2027.
[25] H. Yin, X. Li, and J. Lan, "Iterative mid-range with application to estimation performance evaluation," *IEEE Signal Process. Lett.*, vol. 22, no. 11, pp. 2044–2048, Nov. 2015.
[26] T. Schön, "On computational methods for nonlinear estimation," Dept. Elect. Eng., Linköping Univ., Linköping, Sweden, Tech. Rep., 2003.
[27] N. De Freitas, "Rao–Blackwellised particle filtering for fault diagnosis," in *Proc. IEEE Aerosp. Conf.*, vol. 4. Apr. 2002, pp. 1767–1774.
[28] W. Wu, "Target tracking with glint noise," *IEEE Trans. Aerosp. Electron. Syst.*, vol. 29, no. 1, pp. 174–185, Jan. 1993.
[29] X. Rong Li and Y. Bar-Shalom, "Design of an interacting multiple model algorithm for air traffic control tracking," *IEEE Trans. Control Syst. Technol.*, vol. 1, no. 3, pp. 186–194, Sep. 1993.
[30] E. Daeipour and Y. Bar-Shalom, "An interacting multiple model approach for target tracking with glint noise," *IEEE Trans. Aerosp. Electron. Syst.*, vol. 31, no. 2, pp. 706–715, Apr. 1995.
[31] B.-T. Vo, B.-N. Vo, and A. Cantoni, "Bayesian filtering with random finite set observations," *IEEE Trans. Signal Process.*, vol. 56, no. 4, pp. 1313–1326, Apr. 2008.
[32] T. Hara, M. Mukunoki, I. Tsukamoto, and M. Miyoshi, "Optimization of confirmation time of bistatic tracks in passive radar," *IEEE Trans. Aerosp. Electron. Syst.*, vol. 47, no. 2, pp. 1060–1072, Feb. 2011.
[33] G. Zhou, M. Pelletier, T. Kirubarajan, and T. Quan, "Statically fused converted position and Doppler measurement Kalman filters," *IEEE Trans. Aerosp. Electron. Syst.*, vol. 50, no. 1, pp. 300–318, Jan. 2014.
[34] X. Fan, G. Fan, and J. P. Havlicek, "Generative model for maneuvering target tracking," *IEEE Trans. Aerosp. Electron. Syst.*, vol. 46, no. 2, pp. 635–655, Feb. 2010.

JINGXIAN LIU received the B.S. and M.S. degrees from the China University of Geosciences, Beijing, in 2007 and 2010, respectively. He is currently pursuing the Ph.D. degree in the school of Electrical and Information Engineering, Beihang University, Beijing, China. His research interests include radar tracking and information fusion.

ZULIN WANG (M'14) received the B.S. and M.S. degrees in electronic engineering and the Ph.D. degree from Beihang University, Beijing, China, in 1986, 1989, and 2000, respectively. He is currently the Dean of the School of Electronic and Information Engineering with Beihang University. He has authored or co-authored over 100 papers and published two books in his research fields. He holds six patents. He has undertaken approximately 30 projects related to image/video coding and image processing. His research interests include image processing, electromagnetic countermeasure, and satellite communication technology.

MAI XU (M'10–SM'17) received the B.S. degree from Beihang University in 2003, the M.S. degree from Tsinghua University in 2006, and the Ph.D. degree from the Imperial College London in 2010. From 2010 to 2012, he was a Research Fellow with the Electrical Engineering Department, Tsinghua University. Since 2013, he has been with Beihang University, as an Associate Professor. From 2014 to 2015, he was a Visiting Researcher with MSRA. He has authored over 70 technical papers in international journals and conference proceedings. His research interests mainly include visual communication and image processing. He was a recipient of best paper awards of two IEEE conferences.